RADIO SCIENCE, VOL. 42, RS2008, doi:10.1029/2006RS003485, 2007

Effect of ducting on radio occultation measurements: An assessment based on high-resolution radiosonde soundings

C. O. Ao[1]

Received 21 February 2006; revised 27 November 2006; accepted 1 December 2006; published 28 March 2007.

[1] Recent studies have shown that the presence of elevated ducts in the lower atmosphere has an adverse effect on the inversion of GPS radio occultation data. The problem arises because the microwave refractivity within and below an elevated duct is no longer uniquely determined by the bending angle profile. Applying Abel inversion without a priori knowledge of the duct will introduce a negative bias in the retrieved refractivity profile within and below the duct. In this work, high vertical resolution radiosonde data are used to give a quantitative assessment of the characteristics and effects of ducts, including their frequency of occurrences, heights, and thicknesses at different latitudes and seasons. The negative bias from the Abel-retrieved refractivity profiles resulting from these ducts is also computed. The results give a strong indication that ducting in the lower troposphere is a frequent phenomenon over the tropics and midlatitudes. The ducts are shown to be predominantly caused by sharp changes in the vertical structure of water vapor. The majority of the ducts are found to be below 2 km, with a median duct layer thickness of about 100 m. The negative refractivity bias is shown to be largest below 2 km, with a median value of about 0.5–1% in the tropics and 0.2–0.5% in midlatitudes. The bias is about a factor of 2–3 smaller between 2 to 3 km and is negligible above 4 km.

Citation: Ao, C. O. (2007), Effect of ducting on radio occultation measurements: An assessment based on high-resolution radiosonde soundings, *Radio Sci.*, *42*, RS2008, doi:10.1029/2006RS003485.

1. Introduction

[2] GPS radio occultations (RO) are active limb sounding measurements that yield vertical profiles of refractivity, temperature, and water vapor [*Kursinski et al.*, 1997]. GPS signals used in these measurements operate in the L band frequencies that are insensitive to clouds and precipitation [*Solheim et al.*, 1999]. This feature has been considered to be one of the primary strengths of the technique, enabling RO measurements to probe deep in the planetary boundary layer (PBL), even in regions with heavy cloud covers. Recent advances in retrieval methodology based on wave optics [*Gorbunov*, 2002; *Jensen et al.*, 2003] have greatly improved the accuracy and vertical resolution of GPS RO retrievals. Freed from the constrain of Fresnel diffraction, vertical resolution on the order of 50 m is now theoretically achievable [*Gorbunov et al.*, 2004].

[3] Despite the promise of the technique, recent studies have revealed certain limitations that make RO measurements and retrievals less reliable in the lower troposphere, especially in the moist tropics. There exists two distinct kinds of problems, both of which arise from the presence of fine-scale vertical structures. The first problem comes from the difficulty in acquiring the GPS carrier signals with phase-locked loops, which often fail in the lower troposphere where signal-to-noise ratio is low and the signal bandwidth is high [*Sokolovskiy*, 2001; *Ao et al.*, 2003; *Beyerle et al.*, 2003]. As a result, a significant fraction of the retrieved RO profiles in the tropics and midlatitude regions fail to penetrate into the PBL [*Hajj et al.*, 2004; *von Engeln et al.*, 2005]. This problem, while serious, is expected to be fully resolved in the near future as GPS occultation receivers transition from closed-loop to open-loop tracking in its acquisition mode.

[4] The second problem comes from the failure of Abel inversion when ducting layers (also referred to as

[1]Jet Propulsion Laboratory, California Institute of Technology, Pasadena, USA.

superrefraction or critical refraction layers) are present [*Ao et al.*, 2003; *Sokolovskiy*, 2003]. These ducting layers are caused by the presence of fine refractivity layers with large negative gradients ($dN/dr \lesssim -157$ N-units per km). Examination of the selected tropical radiosonde profiles in the aforementioned studies showed evidence that ducting conditions could occur frequently in the lower troposphere. This is consistent with past studies that focus on the prevalence and the effects of elevated and surface ducts on the long-distance propagation of radio communication signals [*Purves*, 1974; *Patterson*, 1982]. In particular, *Patterson* [1982] catalogues an impressively detailed compilation of global ducting statistics based on five years of radiosonde data (1966–1969, 1973–1974). Nevertheless, it remains unclear how much impact ducting has on GPS RO retrievals across the globe. Basic questions such as the height dependence and the magnitude of the refractivity bias that result from ducting and their spatial-temporal variations have not been addressed.

[5] An interesting study on the effect of ducting has recently been performed based on the European Centre for Medium-Range Weather Forecasts (ECMWF) analysis for a 10 day period in May 2001 [*von Engeln et al.*, 2003] (hereinafter referred to as VNT03). On the basis of the locations of the simulated occultations in this period, the study examined how often an occultation is affected by ducting as well as the height and thickness distributions of the ducts. It was reported that only 10% of the simulated occultation profiles showed ducts and that no ducts were found above 2.5 km altitude. This study was subsequently expanded with the construction of a ducting climatology using six years of ECMWF analysis data [*von Engeln and Teixeira*, 2004] (hereinafter referred to as VT04), providing extremely valuable information on ducting statistics across the globe. However, the use of analysis in constructing the climatology has its limitations. First, the relatively coarse vertical resolution of the ECMWF analysis used (>200 m above 1 km altitude) allows only for the detection of some of the thicker ducts. Thus results from such a study are expected to underestimate the impact of ducting. Second, it is not clear how accurate such fine-scale structures are being represented in the model. Furthermore, the magnitude of the negative refractivity bias, the key consequence of ducting on RO retrievals, was not considered by VNT03 and VT04.

[6] The present work presents a systematic assessment of the impact of ducting on GPS RO measurements using a large number of U.S. high-resolution radiosonde soundings. Even though radiosonde soundings have limited spatial-temporal sampling and are not available routinely over the ocean, it provides reliable temperature and humidity profiles with very high vertical resolution for our investigation.

[7] In section 2, we describe the data set and the methodology used in this study. Statistics of the ducts including duct occurrence frequency, heights, and widths are presented in section 3. Section 4 discusses the negative bias in the retrieved refractivity resulting from the ducts. Section 5 addresses how the results will be affected by the horizontal inhomogeneity of the ducts. The main findings are summarized in section 6.

2. Data and Analysis

[8] The determination of ducts from refractivity profiles depends sensitively on the vertical resolution of the profiles. For this reason, we use the U.S. 6-s radiosonde data that are freely available from the SPARC data center (http://www.sparc.sunysb.edu/html/hres.html) [*Wang and Geller*, 2003]. The radiosonde profiles in this archive are particularly useful for this study because they retain the very high vertical resolution of ≈30 m, which is much better than the mandatory levels in standard radiosonde archives. While some fine-scale vertical structures can be captured by the significant levels that are recorded in the standard radiosonde data set, this is not always sufficient (Figure 1). In choosing the higher-resolution data set over the standard data set, some spatial coverage has been sacrificed in exchange for a higher fidelity in duct characteristics.

[9] The U.S. radiosonde stations from SPARC are primarily located in the Northern midlatitudes, but a number of tropical and high-latitude stations are also included. The soundings are available twice daily at 00 and 12 hours UTC. We use data from the years 2001–2004, which have routine measurements from 86 stations. Among them, 14 are located in the tropics (30°S–30°N), 60 are located in midlatitudes (30°N–50°N), and 12 are located at high latitudes (>50°N). The data are used as is without any additional quality control.

[10] The refractivity profile can be constructed from the temperature, pressure, and humidity profiles of a radiosonde sounding as follows [*Smith and Weintraub*, 1953]:

$$N(r) = a_1 \frac{P(r)}{T(r)} + a_2 \frac{P_w(r)}{T^2(r)} \tag{1}$$

where T is the temperature (K), P is the total pressure (mb), and P_w is the water vapor partial pressure (mb). The coefficients are $a_1 = 77.6$ K mbar^{-1} and $a_2 = 3.73 \times 10^5$ K^2 mbar^{-1}. The refractive index is related to the refractivity through the expression $N = (n - 1) \times 10^6$.

[11] In a spherically symmetric atmosphere and under the laws of geometric optics, the ray's trajectory is confined to a plane and is described in polar coordinates (r, θ) by [e.g., *Born and Wolf*, 1999]

$$\frac{d\theta}{dr} = \frac{a_o}{r} \frac{1}{\sqrt{n^2 r^2 - a_o^2}} \tag{2}$$

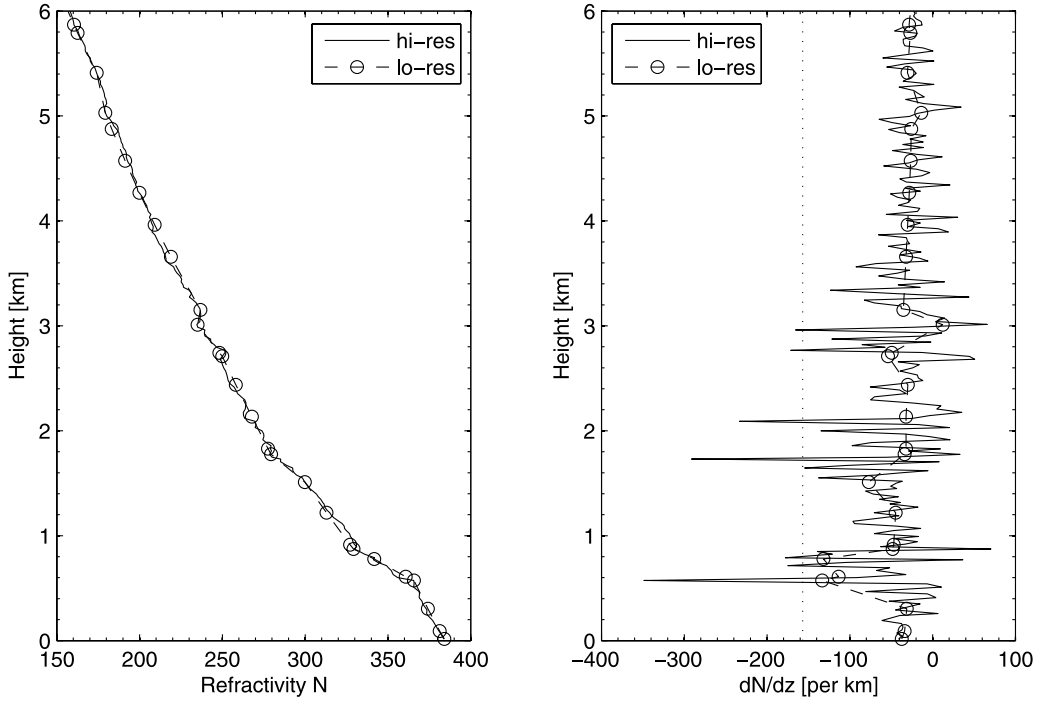

Figure 1. Comparison between refractivity profiles derived from the high-resolution ("hi-res") and standard ("lo-res") radiosonde data. Even though the significant levels of the standard radiosonde data capture the sharp changes in the refractivity profile reasonably well, the additional levels from the high-resolution data are needed to bring out the ducts quantitatively (places where the vertical refractivity gradient $dN/dz < -157$ per km). This particular example is taken from the sounding at Yap Island (9.48°N, 138.08°E) on 22 January 2004, 1200 UT. The standard radiosonde profile was downloaded from the University of Wyoming Web site http://weather.uwyo.edu/upperair/sounding.html.

where $a_o = n(r_o)r_o$ is a constant, with r_o being the tangent point radius. In the Earth's atmosphere, the function $a(r) \equiv n(r)r$ usually increases monotonously with r, i.e., $a' \equiv da/dr > 0$. The dominator in equation (2) implies that the ray is defined for $r > r_o$ and that the ray's tangent point radius is also its minimum radius. The bending of the ray from its tangent point to outside the atmosphere is obtained by integrating over (2), i.e., $\int d\theta - \pi/2$, giving

$$\alpha_{1/2}(a_o) = -a_o \int_{r_o}^{\infty} \frac{dr}{\sqrt{a^2 - a_o^2}} \frac{d\ln n}{dr} \qquad (3)$$

[12] Since the transmitter and receiver are located far from the atmosphere in a GPS RO, the total bending from transmitter to receiver is $\alpha = 2\alpha_{1/2}$. When $a'(r) > 0$ for all $r > r_o$, there is a one-to-one relationship between a and r. This allows one to express $n(r)$ and consequently the integrand in equation (3) as a function of a. In this way, the integral can be directly inverted to yield $n(a)$ as an integral over $\alpha(a)$—the well-known Abel inversion integral which serves as the basis for RO retrievals. (See section 4 for more details.)

[13] A duct or "trapping layer" exists in the atmosphere when the refractive index decreases so rapidly with height that $a'(r) < 0$. Figure 2 shows a schematic example where $a'(r)$ for $r_m < r < r_t$. A ray with its tangent point radius greater than r_t will not see this region and will bend as governed by (3) in reaching outside the atmosphere. However, a ray with its tangent point radius in the region $r_b < r_o < r_t$ encounters turning points within this layer where $a = a_o$ and $dr/d\theta = 0$. Thus the ray becomes trapped inside this layer or duct. For $r_o < r_b$, the tangent point falls below the duct; with $r > r_o$, $a > a_o$, the ray is no longer trapped so that equation (3) is once again applicable. The ducting condition $a' < 0$ is equivalent to $n' < -n/r$, or $N' \lesssim -157$ per km since $n \approx 1$ and $r \approx 6370$ km.

[14] Of course, in an occultation geometry, the ray is never trapped inside the atmosphere since a trapping ray by definition could never reach outside the atmosphere. For GPS RO, the problem with the presence of a duct is the nonexistence of tangent point within a duct for rays

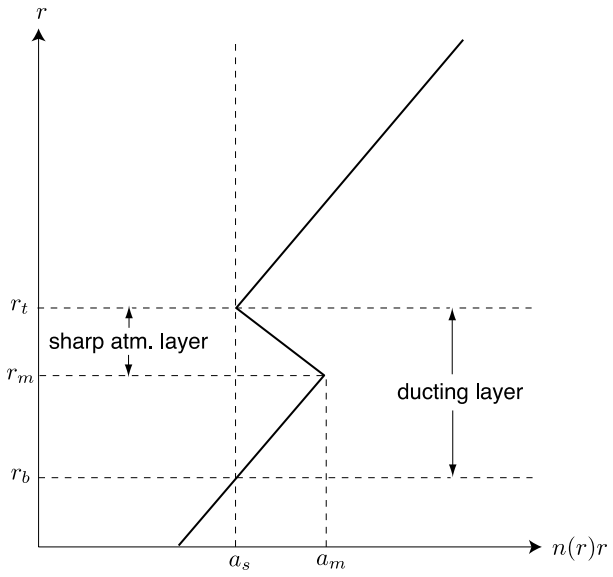

Figure 2. Schematic illustration of an elevated duct.

that reach outside the atmosphere. The fact that the transformation between a and r breaks down when duct exists means that Abel inversion of the bending angle to obtain refractivity will fail in this region. Indeed, when duct exists, there is no longer a one-to-one relationship between the bending angle profile $\alpha(a)$ and refractive index profile $n(r)$ [*Sokolovskiy*, 2003]. An infinite number of refractive index profiles—of which the Abel inversion offers but one possibility—that differ only within and below the duct can be shown to give an identical $\alpha(a)$ (see Appendix A).

[15] Note that the duct is defined here as the layer $r_b < r < r_t$ because this is the region where rays are trapped, even though $a' < 0$ only for $r_m < r < r_t$, where the sharp changes in refractivity occur. The latter condition is commonly used in defining the duct layer (e.g., VTN03 and VT04). However, the former is preferred here because it is more relevant to signal propagation and the associated effect on the retrieval. Thus the duct thickness presented here will always be greater than the value obtained from its common definition, with a difference of $r_m - r_b$.

[16] The steps for finding ducts from each radiosonde sounding are as follows:

[17] 1. Obtain refractivity profile $N(r)$ and interpolate $N(r)$ to a regular grid with 1 m spacing.

[18] 2. Compute $a(r)$ between 0 to 10 km.

[19] 3. Check the value of $a'(r)$ from the top down. When $a'(r) < 0$, we have found the top of a duct r_t.

[20] 4. When $a'(r) > 0$, we have found r_m, the "middle" of the duct.

[21] 5. When $a(r) = a(r_t)$, we have found r_b, the bottom of the duct.

[22] If the bottom of the profile is reached before the conditions in step (3) and/or step (4) are reached, the duct is a surface duct, with $r_b = r_s$. Otherwise, continue the steps (3)–(5) below r_b until all ducts are found. It is useful to keep track of both r_m and r_b for a duct because the former gives information on the sharp layer and is related to the physical processes or conditions that form the ducts, while the latter gives information on the vertical extent of the duct and is related to its impact on the inversion of RO measurements.

[23] Key parameters for the duct are the duct height z_t, the duct layer thickness $d = r_t - r_b$, and the change of refractivity, temperature, and water vapor across the sharp layer that leads to the duct. In the next section, the frequency of occurrence of ducts as well as the spatial-temporal characteristics of the duct parameters are discussed.

3. Duct Statistics

3.1. Frequency of Occurrences

[24] We first examine how frequently ducting occurs in the lower troposphere and how the frequency of ducting varies monthly and geographically. For each month and at each radiosonde station, we count the number of profiles that contain at least one ducting layer (n_d) and divide it by the total number of profiles (n_t). For this purpose, ducts with small $\Delta N = N(r_b) - N(r_t)$ will not be counted. In general, ΔN is found to correlate strongly with the thickness of the duct d. A cutoff threshold of $\Delta N = 5$, which corresponds to $d \approx 30$ m, is chosen. This cutoff is imposed for several reasons. First, ducts with small ΔN have more minor impact on GPS RO retrievals. Second, ducts with thicknesses less than the vertical resolution of the radiosonde profiles are less reliably determined. Third, small ducts likely reflect more localized conditions, with horizontal extent much smaller compared to the horizontal resolution of the measurement. The effects from such small-scale horizontal and vertical inhomogeneities are different from ducting [e.g., *Sokolovskiy*, 2003] and are best treated as a random process [e.g., *Ishimaru*, 1978].

[25] Figure 3 shows the monthly distributions of the ducting frequency, which are found to cluster into three groups. The first cluster, consisting of tropical stations as well as those along the California and Gulf coasts, shows ducting frequency over 60% year round. The second cluster, consisting of midlatitude stations to the east of the Rocky Mountains and in the Pacific Northwest, shows a strong seasonal dependence, with very frequent ducting in the Northern Hemisphere (NH) summer and infrequent ducting in the winter. The third cluster, consisting of inland midlatitude stations to the west of the Rocky Mountains and high-latitude stations, shows a

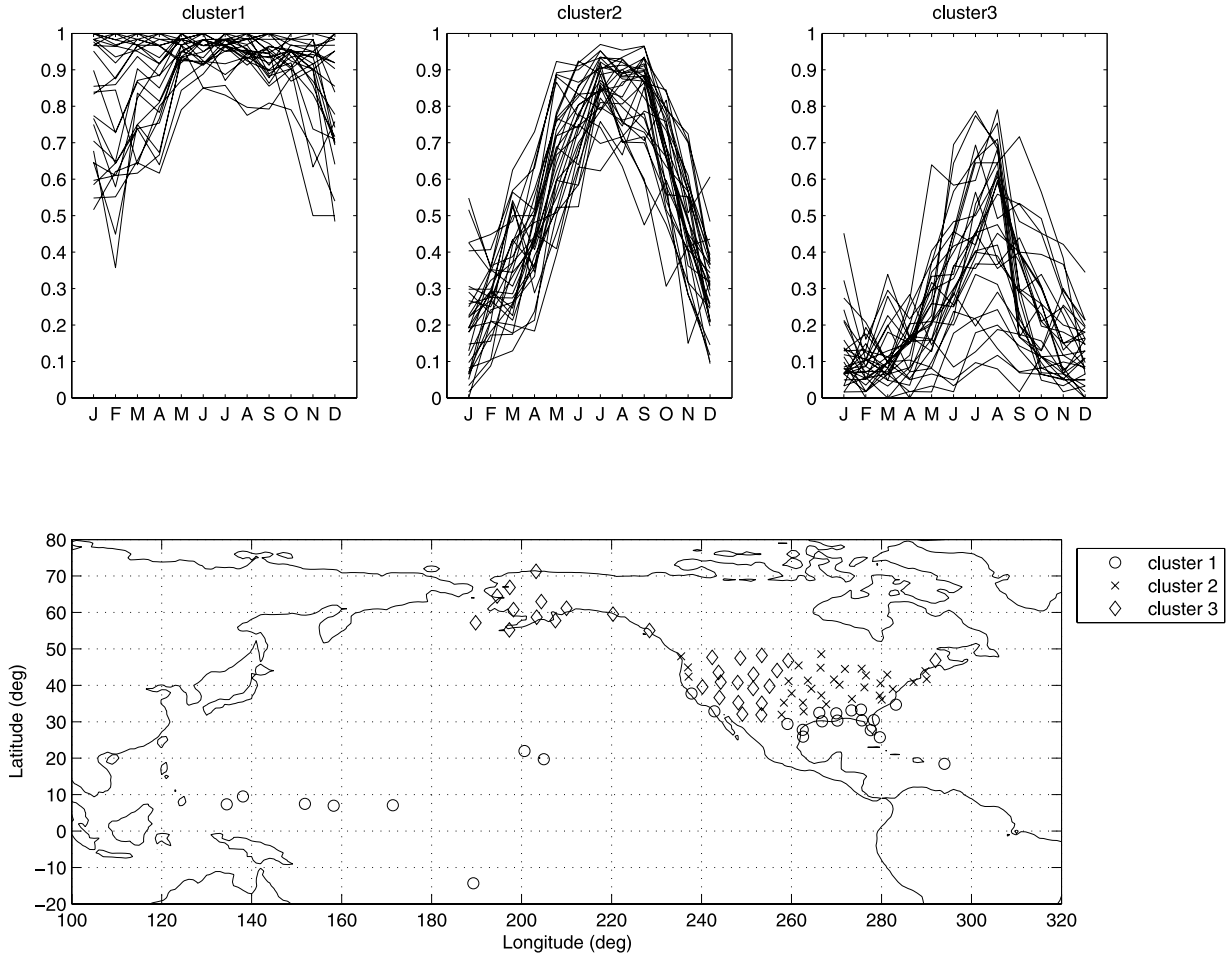

Figure 3. Frequency of ducting occurrences in a year. Cluster analysis shows that the frequency plots can be divided into three groups.

more abrupt transition from winter to summer, with very little ducting except during the summer months.

[26] The high frequency in the occurrence of ducts as evidenced by Figure 3 contrasts sharply with the 10% value reported by VNT03, although the more extensive analysis by VT04 does shows nearly 100% ducting probability off the west coasts of the American, African, and Australian continents. In general, the ducting frequency from the ECMWF analysis appears to show a rather dramatic "feast or famine" distribution where the ducting probability is either very high or very low. This pattern of duct frequency distribution is not apparent from the radiosonde analysis.

3.2. Water Vapor Versus Temperature

[27] The monthly dependence and geographical distribution of ducting frequency as shown in Figure 3 appears to be correlated with the distribution of water vapor in the lower troposphere. To investigate this point further, we consider the fraction of refractivity change which is due to a change in water vapor. The sharp refractivity change that is responsible for the formation of the duct can be caused by a sharp change in water vapor and/or temperature. From equation (1),

$$\Delta N_s = a_1 \frac{\Delta P}{T} - \left(a_1 P + 2a_2 \frac{P_w}{T} \right) \frac{\Delta T}{T^2} + a_2 \frac{\Delta P_w}{T^2} \equiv \Delta N_P + \Delta N_T + \Delta N_w \quad (4)$$

where $\Delta N_s = N(r_m) - N(r_t)$, which is large and positive for a duct. (Note that ΔN_s is different from ΔN, which is the difference in refractivity between r_b and r_t). The corresponding pressure, temperature, and water vapor partial pressure changes are $\Delta P = P(r_m) - P(r_t)$, $\Delta T = T(r_m) - T(r_t)$, $\Delta P_w = P_w(r_m) - P_w(r_t)$, respectively.

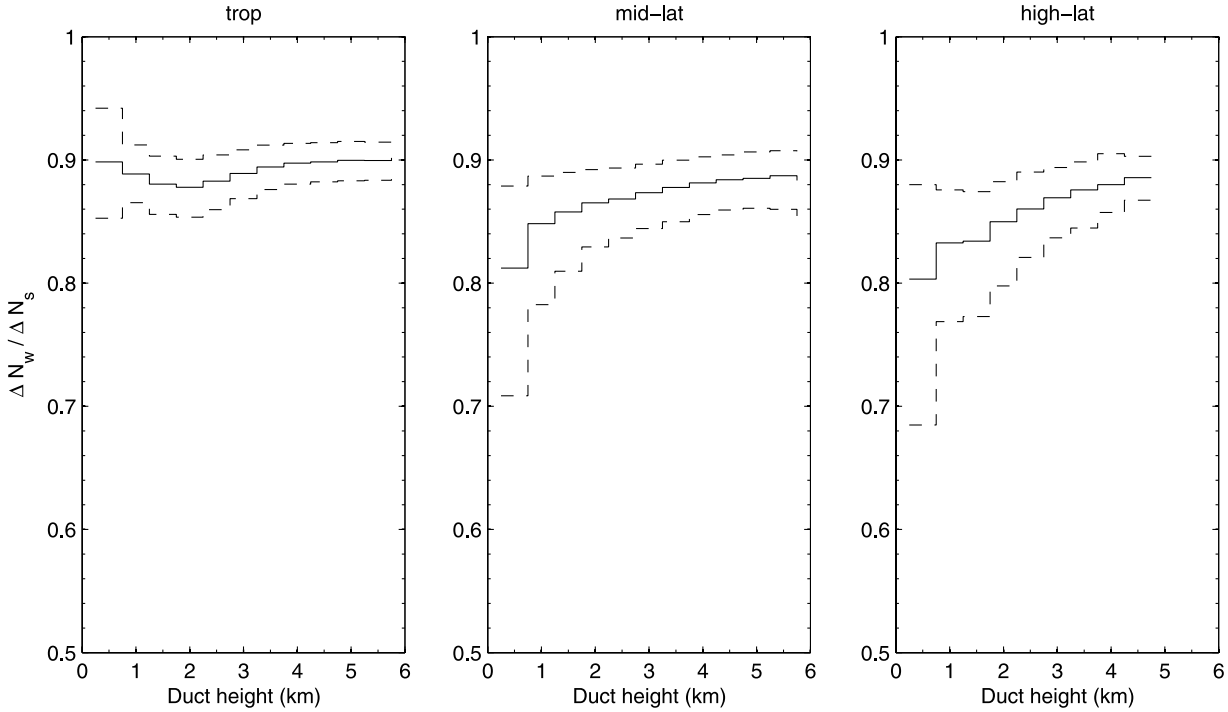

Figure 4. Contribution of water vapor change to the formation of a duct, shown as the fraction of refractivity change due to a change of water vapor $\Delta N_w/\Delta N_s$. Solid line represents the median over four years of data, and dashed lines represent the 25th and 75th percentiles.

The first term ΔN_P in (4) is due to the increase in pressure from r_t to r_m as controlled by hydrostatic equilibrium and typically accounts for only 10%–20% of ΔN_s in a ducting layer. The second term ΔN_T is usually small but can have a significant and positive contribution to ΔN_s in a strong inversion layer where $\Delta T < 0$. The third term ΔN_w is due to a change of water vapor partial pressure.

[28] Figure 4 presents the statistics of $\Delta N_w/\Delta N_s$ as a function of ducting height z_t for different latitude bands averaged over 2001–2004. The median as well as the 25th and 75th percentile values are shown. For all latitude bands, the refractivity change responsible for ducting is almost entirely due to the change in water vapor. In midlatitude and high-latitude stations, temperature change has a slightly more important contribution to the formation of ducts close to the surface.

[29] Similar conclusion can be drawn from Figure 5, which shows the median as well as the 25th and 75th percentiles for the changes in specific humidity Δq and temperature ΔT that lead to ΔN_w and ΔN_T, respectively. Overall, Δq is largest in the tropics (2–3 g/kg) and tapers off as latitude increases. As for the temperature change, ΔT is nearly zero in the tropics but its magnitude increases for the midlatitudes and high latitudes (generally less than 1 K). It is interesting to note that one midlatitude station (“Miramar NAS” near San Diego) stands out from the rest as having the largest Δq at 4 g/kg and $-\Delta T$ at 1.5 K. Thus the largest ducts (i.e., the duct with the largest ΔN) are found at this location among all the stations. In fact, it is well known that very strong elevated layers could form in this region because of large-scale subsidence coupled with the föhn-like Santa Ana winds that bring especially warm and dry air over the cool and moist marine air [*Gossard and Strauch*, 1983; *Purves*, 1974].

3.3. Ducting Layer Height and Thickness

[30] The heights and thicknesses of the ducting layers are key parameters that relate not only to the underlying physical processes that lead to their formation but also directly impact the biases in RO retrievals. Because multiple ducts are often present in a profile, it is not possible to assign just one value of height and thickness to each profile. Thus for each profile, three categories of ducts are considered: (1) the highest duct, (2) the lowest duct, and (3) the largest duct (i.e., the duct with the largest ΔN). Obviously for profiles with a single duct, the three kinds of ducts are the same.

[31] Figure 6 (top) shows the four-year median value of the duct height z_t at each station. The circle indicates

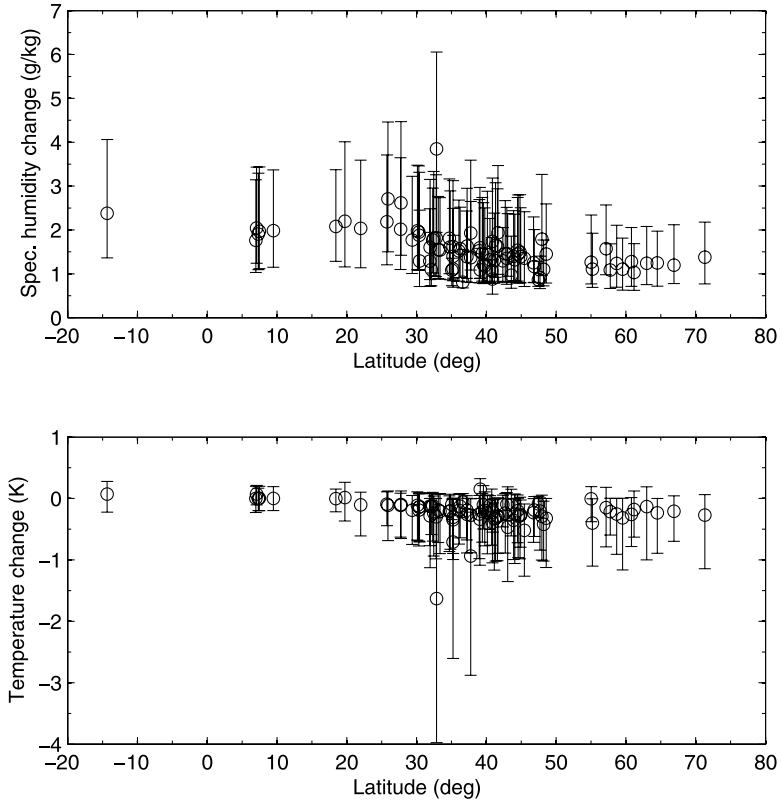

Figure 5. Changes of water vapor and temperature across the sharp layers that form ducts. The circles show the median values at each radiosonde station, while the top and bottom error bars show the 75th and 25th percentiles, respectively.

the median value for the largest duct. The top and bottom error bars indicate the median values of the highest and lowest ducts, respectively. Overall, the ducting heights are mostly between 1–2 km altitude for the tropical and midlatitude stations and at about 1 km altitude for the high-latitude stations. The tropical stations, with the largest number of multiple ducts, show the largest variance in ducting heights, with a median value of 2.5 km for the highest ducts. The spread of the duct height is in the range of 0.5 to 1 km, due to diurnal and seasonal variability (not shown). A few midlatitude stations located on inland, high terrains have very high ducts; moreover, they tend to have only one duct. These stations include Grand Junction, CO, Albuquerque, NM, and Desert Rock, NV.

[32] Figure 6 (bottom) shows another view of the duct height distribution. The normalized number of profiles in 0.5 km bins of z_t (based on the largest duct) is computed for different latitude bands. The majority of the ducts occurs below 2 km for all latitude bands. The tropical and midlatitude ducts peak between 0.5 to 1 km, while the high-latitude ducts peak between 0 to 0.5 km. A small fraction of the ducts occur as high up as 4 km. In contrast, no ducts above 2.5 km were reported by VNT03; they were not considered at all by VT04 because of the coarser vertical resolution of the ECMWF analysis at higher altitudes.

[33] Next we examine the thickness of the ducts. For simplicity, only the largest ducts are considered. Figure 7 (top) shows the median duct thickness for each station, with the error bars indicating the 25th and 75th percentiles. The tropical profiles generally have the thickest ducting layer with a median thickness between 100 to 200 m. The midlatitude profiles have median thicknesses mostly at or below 100 m, while high-latitude profiles have median values below 100 m. The station with the largest median thickness is at Miramar NAS, where the ducts have the largest Δq and $-\Delta T$ (see section 3.2 and Figure 5). Figure 7 (bottom) shows the height distribution of the duct thicknesses. Generally, the ducts are found to be thickest near 1–2 km and become slightly thinner at heights above or below this range. Because of

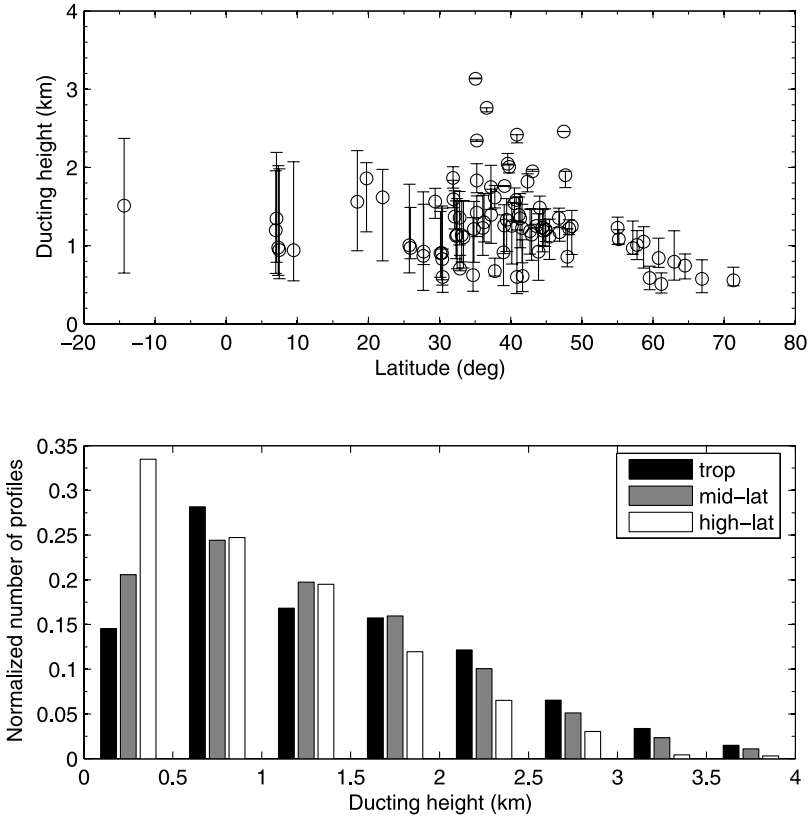

Figure 6. Statistics of duct heights. (top) Circles represent median values of the largest ducts at each radiosonde station. The top (bottom) error bars represent the median values of the highest (lowest) ducts. (bottom) Distribution of duct heights.

the strong correlation between duct thickness and ΔN, the thickness distribution shown in Figure 7 can be used to infer the distribution of ΔN.

[34] Figure 8 shows the monthly variation of the median duct heights and thicknesses for different latitude bands. An annual cycle of amplitude less than 0.5 km in the duct height and less than 30 m in the duct thickness can be inferred. It is interesting to note that the midlatitude and high-latitude profiles have higher and thicker ducting layers during the NH summer months, while the tropical profiles have the opposite trend.

4. Refractivity Bias

[35] The existence of ducts causes a negative bias in the Abel-retrieved refractivity from the top of the ducting layer. In this section, we show how the bias can be computed and present numerical results for the bias as a function of height and month of year for the radiosonde locations.

[36] From equation (3), the bending angle profile $\alpha(a)$ is given in terms of the input refractive index $n(r)$ (or equivalently input refractivity $N(r)$) by

$$\alpha(a_o) = -2a_o \int_{r_o}^{\infty} \frac{dr}{\sqrt{(n(r)r)^2 - a_o^2}} \frac{d\ln n}{dr} \qquad (5)$$

[37] In the absence of ducts, there is a one-to-one relationship between $a = n(r)r$ and r. A change of variable from r to a in equation (5) gives

$$\alpha(a_o) = -2a_o \int_{a_o}^{\infty} \frac{da}{\sqrt{a^2 - a_o^2}} \frac{d\ln n}{da} \qquad (6)$$

[38] This can be inverted via Abel transform to yield the retrieved refractive index n_a

$$\ln n_a(a_o) = \frac{1}{\pi} \int_{a_o}^{\infty} da \frac{\alpha(a)}{\sqrt{a^2 - a_o^2}} \qquad (7)$$

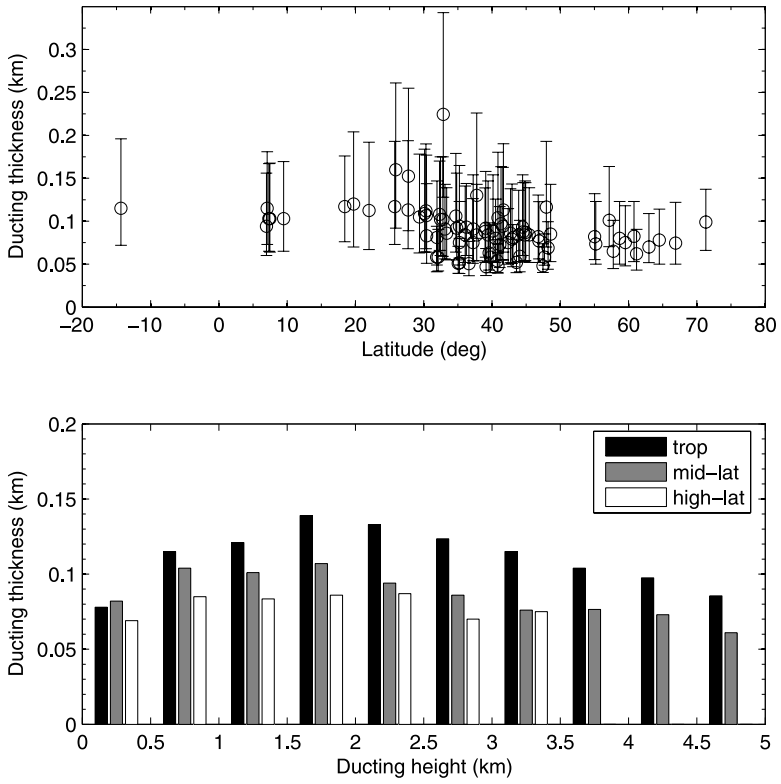

Figure 7. Statistics of duct thicknesses. (top) Median and 25th and 75th percentile values at each radiosonde station. (bottom) Distribution of duct thicknesses as a function of height.

[39] When ducts are absent, the Abel-retrieved refractivity N_a reproduces the input refractivity N. When ducts are present, equation (5) is still valid, but equation (6) is not. In this case, the Abel-retrieved refractivity can be related to the input refractivity as (see Appendix A)

$$N_a(a_o) - N(a_o) = \begin{cases} 0, & a_o > a_s \\ -\Delta N + I_d(a_o), & a_o \le a_s \end{cases} \quad (8)$$

where $a_s = n(r_t)\ r_t = n(r_b)\ r_b$ denotes the impact parameter where the duct occurs (cf. Figure 2). The function $N(a_o) = N(r_o n(r_o))$ is defined only for $r_o < r_b$ ($a \le a_s$) or $r_o > r_t$ ($a > a_s$). The function $I_d(a_o)$ is zero at the duct ($a_o = a_s$) and approaches ΔN asymptotically with decreasing a_o. It follows that the difference $N_a(a_o) - N(a_o)$ is minimum at the duct (equal in value to $-\Delta N$) and approaches zero at a_o sufficiently far below the duct. Equation (8) can be easily generalized to the case of multiple ducts.

[40] Equation (8) gives the refractivity difference as a function of a_o. However, the refractivity profile is usually expressed as a function of r_o. To obtain the refractivity difference as a function of r_o, first compute $N_a(a_o)$ from equation (8). Next, obtain the corresponding tangent point radius by $r_o = a_o/n_a(a_o)$; this gives the function $N_a(r_o)$. From this, the difference $N_a(r_o) - N(r_o)$ can be calculated. The results below will be presented in terms of the fractional refractivity bias, defined as $(N_a(r_o) - N(r_o))/N(r_o)$.

[41] Figure 9 shows the median of the fractional refractivity error for each station altitude ranges of 0–1 km, 1–2 km, 2–3 km, and 3–4 km, with error bars indicating the 25th and 75th percentiles. Because of the more frequent ducting and thicker ducting layers in the tropics, the negative bias is largest there, with a median of 0.5–1% below 2 km. In midlatitude stations, the negative bias is slightly smaller, at about 0.2–0.5% below 2 km. The bias is negligible at high-latitude stations. The interquartile range (IQR, defined as the difference between the 75th and 25th percentiles) reflects the significant temporal variability of the ducts, is largest when the negative bias is largest. In the tropics, the IQR is found to be up to 1–2% below 2 km.

[42] The monthly median and IQR values of the fractional refractivity bias for different latitude bands at the height range of 0–2 km are shown in Figure 10. The negative bias is largest for the midlatitude and high-latitude profiles in the NH summer and smallest in the

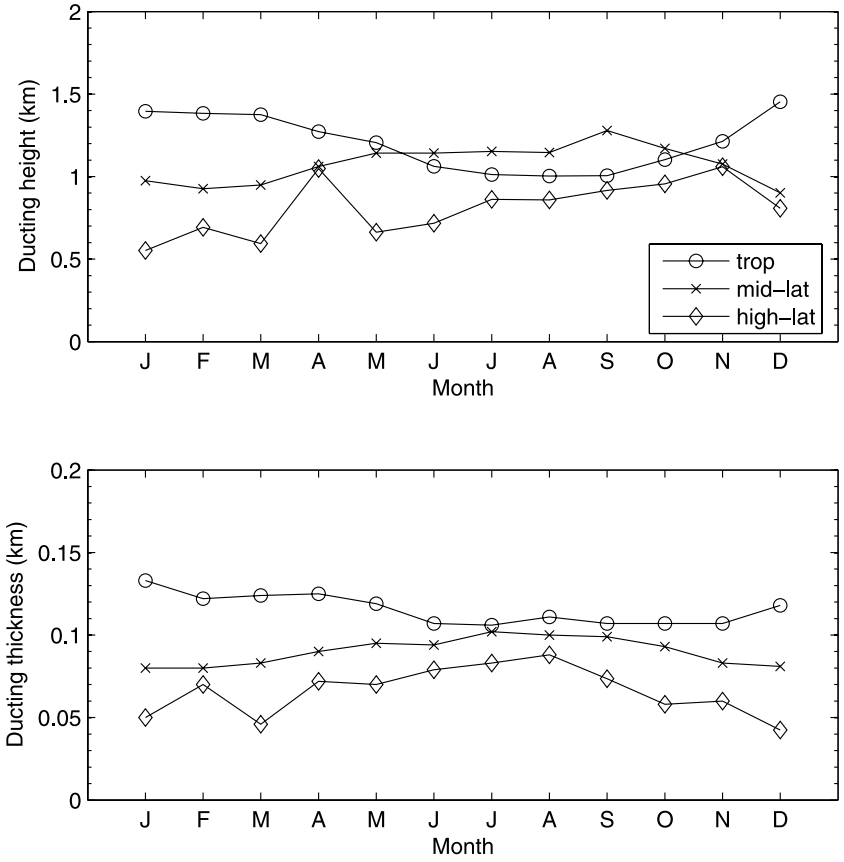

Figure 8. Monthly variation of median duct heights and thicknesses for different latitude bands.

winter. The opposite is true for the tropical profiles, although the seasonal amplitude is smaller. These trends mirror the seasonal dependence of the duct thicknesses and heights (cf. Figure 8). The negative biases from the tropical and midlatitude profiles are comparable in the summer and differ greatly in the winter. Similar to Figure 9, the IQR is shown to be positively correlated with the negative bias, meaning that the variability is largest where the negative bias is largest.

5. Discussion of Horizontal Inhomogeneity

[43] The use of radiosonde profiles in evaluating the refractivity bias due to ducts has a serious drawback. Radiosonde sounding gives local measurements and do not yield information about the horizontal variation of the ducts. GPS RO measurements, on the other hand, are nonlocal and depends on both the horizontal and vertical gradients of the refractivity along the signal path. Typically, the data are inverted under the assumption of local spherical symmetry (LSS), with the retrieved value of refractivity attributed to the tangent point of the ray. "Local" refers to a horizontal extent of $\pm\sqrt{2r\Delta r}$ around the tangent point with radius r and vertical extent of Δr [*Kursinski et al.*, 1997; *Ahmad and Tyler*, 1998]. Considering a duct with thickness of 100 m, which is approximately the median thickness of ducts (cf. Figure 7), its horizontal extent should cover at least ±35 km or ±0.31° for LSS to hold. A thicker duct would need to be more horizontally homogeneous since the horizontal distance traversed by the ray while within this layer is larger.

[44] To illustrate the effect from the horizontal inhomogeneity of a duct, a simple two-dimensional (2-D) model is constructed, where a profile with a duct $N_1(r)$ is confined within an horizontal extent of $\pm\Delta\theta$. Outside this angular range, the refractivity smoothly transitions to the "background" profile $N_2(r)$, which has no ducts. The bending angle is computed by ray tracing through this 2-D medium. Abel inversion of the bending angle then gives the retrieved refractivity profile $N^{(inv)}(r)$. This retrieved refractivity can then be compared with $N_1(r)$, $N_2(r)$, as well as $N_1^{(inv)}(r)$, which is the Abel-inverted refractivity profile when the input refractivity is spherically symmetric everywhere and equal to $N_1(r)$.

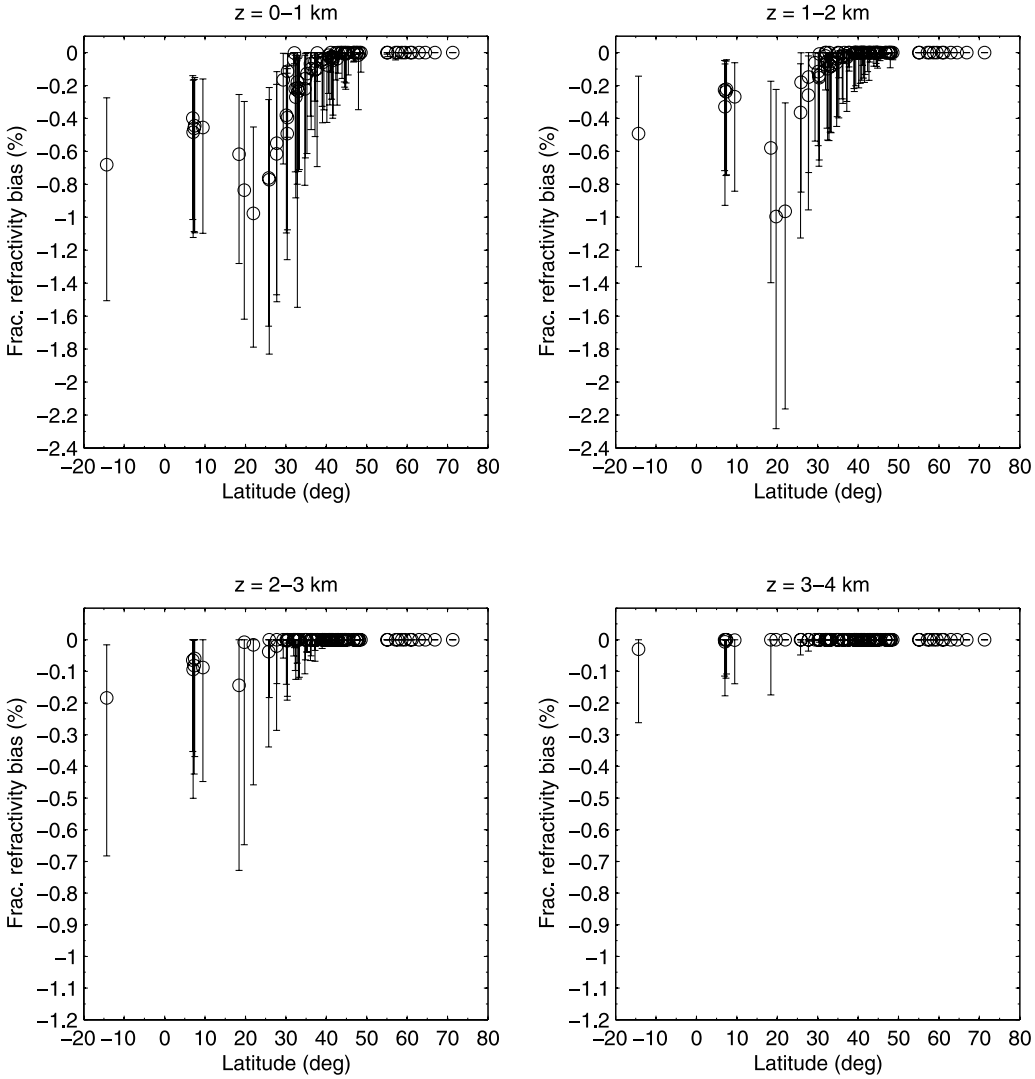

Figure 9. Fractional refractivity bias at each radiosonde station. The circles show the median values, while the top and bottom error bars show the 75th and 25th percentiles, respectively.

[45] Figure 11 shows an example where $N_1(r)$ is obtained from a radiosonde sounding at Greensboro, North Carolina. It has a duct at the height of $z_t = 2.69$ km with a thickness of 183 m and $\Delta N = 28.72$. The background $N_2(r)$ is constructed by removing the points from $N_1(r)$ that lie between 2 to 2.6 km in height and replacing such points with a cubic interpolation. The angular extent of $N_1(r)$ is varied from $\Delta\theta = 0.1°$ to $\Delta\theta = 0.5°$. It can be seen from Figure 11 that with $\Delta\theta = 0.1°$, the retrieved refractivity $N^{(inv)}(r)$ only exhibits a hint of the sharp structure. In this case, $N^{(inv)}(r)$ is clearly closer to $N_2(r)$. With $\Delta\theta = 0.2°$, $N^{(inv)}(r)$ moves closer to $N_1^{(inv)}(r)$. With $\Delta\theta = 0.5°$, the influence of the duct is stronger than the background, and $N^{(inv)}(r)$ nearly overlaps with $N_1^{(inv)}(r)$. According to the LSS assumption, the duct should have a horizontal extent of $\sim\pm 0.43°$ for the spherically symmetric solution to be valid. This is consistent with the results shown in this example.

[46] The results from section 4 have been derived assuming that the ducts are locally spherically symmetric. This is more likely to be true over the tropical island stations than over mountainous terrain. Thus the results derived from high-resolution radiosonde profiles probably overestimate the impact of ducting. Unfortunately, it is very difficult to quantitatively evaluate the horizontal extent of ducts because of the lack of such data. For the radiosonde data used here, the closest pair of stations has a spatial separation of 130 km and is therefore not very

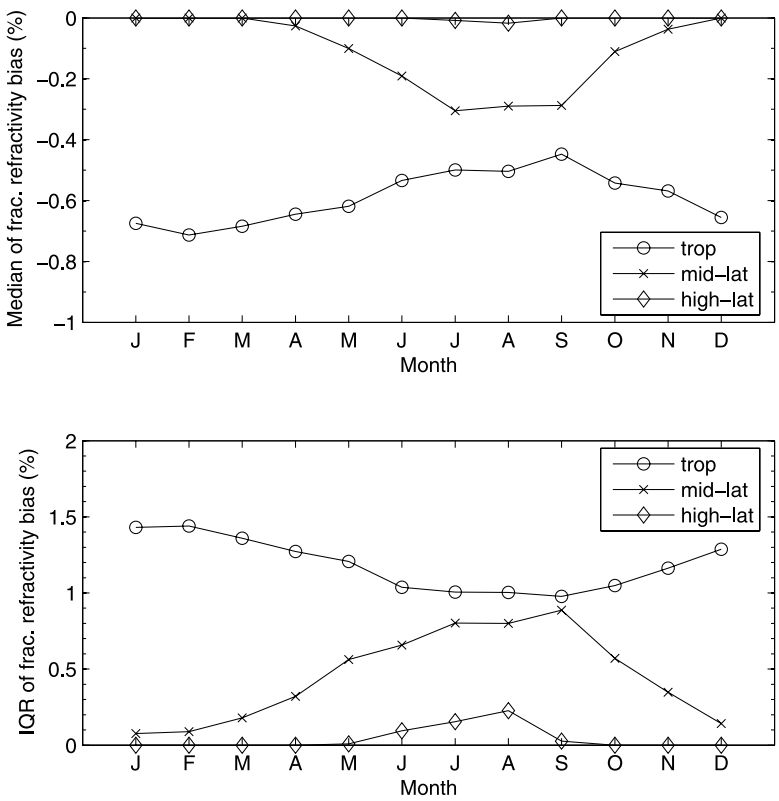

Figure 10. Monthly variation of median and interquartile range (IQR) refractivity bias for different latitude bands at the height range of 0–2 km.

useful for such an evaluation. Despite the uncertainty of horizontal inhomogeneity, the results presented here still yield valuable information on the impact of ducting. At worst, such results can be interpreted as providing an upper bound on the effects of ducting on GPS RO retrievals at these locations.

6. Conclusions

[47] The presence of ducts in the lower atmosphere has a significant impact on radio occultation retrievals. Traditional onion-peeling approach that relies on Abel inversion to retrieve refractivity is no longer valid below a duct. When applied, the inverted refractivity is found to be systematically smaller than the true refractivity. This negative bias is largest just below the duct and decays as the height decreases.

[48] For radio occultation data to be useful in the lower troposphere and the PBL, the following questions need to be addressed.

[49] 1. What is the percentage of occultations that will be affected by ducting? What are the latitude, longitude, and height distributions?

[50] 2. What is the corresponding refractivity bias resulting from ducting?

[51] 3. Can we identify which occultations have been affected by ducting?

[52] 4. Can we retrieve the true refractivity for an occultation affected by ducting?

[53] This paper attempts to shed lights on questions (1) and (2) by using a multiyear, high vertical resolution radiosonde data set. The high vertical resolution is a key in this study because the identification of ducts from a refractivity profile is sensitively dependent on the vertical resolution of the profile. However, the use of the high-resolution radiosonde data has two major drawbacks. First, the data lack global coverage. The radiosonde stations used here are located over land and predominately over the United States. The availability of data over tropical islands helps to provide some information over the marine environment. Unfortunately, a true global climatology such as that from VT04 is not attainable with the use of radiosonde data. Second, radiosonde soundings only provide point measurements. Given the large horizontal separations between the

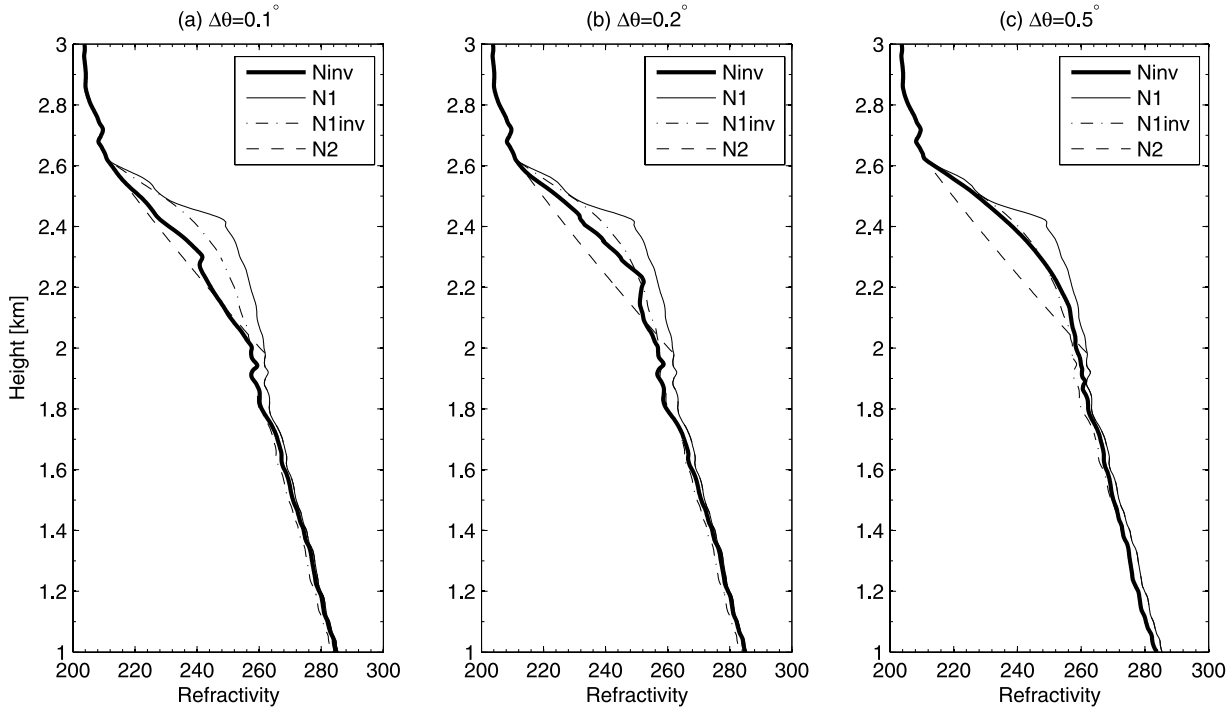

Figure 11. Simple 2-D example showing the effect of horizontal inhomogeneity on GPS RO retrievals. The profile $N_1(r)$ has a duct with width of 183 m and is confined to an angular extent of $\pm\Delta\theta$ around the tangent point. Outside this region, $N_1(r)$ transitions smoothly to a background profile $N_2(r)$ which has no duct. The plot shows that the inverted profile $N^{(inv)}(r)$ becomes closer to the inverted profile $N_1{}^{(inv)}(r)$ (obtained when $N_1(r)$ is globally spherically symmetric) as $\Delta\theta$ increases.

radiosonde stations used here, horizontal variations of the sharp refractivity structures cannot be easily assessed.

[54] Despite these caveats, our results give a strong indication that ducting in the lower troposphere is a frequent phenomenon over the tropics and midlatitudes. The ducts are found to be caused almost entirely by sharp changes in the vertical structure of water vapor. The majority of the ducts are found to be below 2 km with a duct layer thickness of about 100 m. As a result, the negative refractivity bias arising from the presence of the ducts is largest below 2 km, with a median value of about 0.5–1% in the tropics and 0.2–0.5% in midlatitudes. The bias is about a factor of 2–3 smaller between 2 to 3 km and is negligible above 4 km. There are significant seasonal variations in duct characteristics and the resulting negative bias, especially in the extratropics. The negative bias is largest for midlatitude and high-latitude profiles in the summer months, while the opposite is true for the tropical profiles. These results are derived under the assumption of local spherical symmetry. A 100-m duct would need to have a horizontal extent of approximately 70 km for this assumption to be valid. Without knowing the true horizontal extents of ducts, the results presented here can be interpreted more cautiously as yielding an upper bound on the effects of ducting on GPS RO retrievals at these locations.

[55] Questions (3) and (4) are currently active areas of research. A promising approach to invert refractivity in the presence of ducts has recently been proposed [*Xie et al.*, 2006], but more work is needed to validate its effectiveness when applied to real data. Another potentially fruitful approach is to employ a nonlinear optimization method based on the assimilation of bending angles [*Palmer et al.*, 2000; *Zou et al.*, 2000]. This method could work because unlike refractivity, the bending angles derived from RO measurements are in principle not affected by ducting.

[56] Until a reliable way is devised to filter out data affected by ducting or, better yet, to remove the bias from the retrieved refractivity, it is important to take the negative bias from ducting into account when lower troposphere refractivity (or a derived product such as water vapor) is used. It is hoped that the characteristics of the biases derived in this paper could provide some

guidance for a more effective use of RO measurements in the lower troposphere and the PBL.

Appendix A

[57] In this appendix, the expression for the difference between the Abel-retrieved refractivity and the input refractivity in the presence of ducts is derived.

[58] Consider a single ducting layer between r_t and r_b (Figure 2). From equation (5), for $a_o < a_s$, the bending angle is

$$\alpha(a_o) = -2a_o\left[\int_r^{r_b} + \int_{r_b}^{r_t} + \int_{r_t}^{\infty}\right] \frac{dr}{\sqrt{(n(r)r)^2 - a_o^2}} \frac{d\ln n}{dr} \tag{A1}$$

which can be rewritten as

$$\alpha(a_o) = -2a_o\left[\int_{a_o}^{a_s} + \int_{a_s}^{\infty}\right] \frac{da}{\sqrt{a^2 - a_o^2}} \frac{d\ln n}{da} - 2a_o \int_{r_b}^{r_t} \frac{dr}{\sqrt{(n(r)r)^2 - a_o^2}} \frac{d\ln n}{dr} \tag{A2}$$

with the understanding that $n(a)$ is defined on the basis of $\{n(r), r > r_t\}$ for $a > a_s$ and $\{n(r), r < r_b\}$ for $a < a_s$. Note that $n(a)$ as defined is discontinuous at $a = a_s$. It is equal to $n(r_t)$ when approached from above ($a > a_s$) and $n(r_b)$ when approached from below ($a < a_s$).

[59] Let n_a be the Abel-inverted refractive index.

$$\alpha(a_o) = -2a_o \int_{a_o}^{\infty} \frac{da}{\sqrt{a^2 - a_o^2}} \frac{d\ln n_a}{da} \tag{A3}$$

[60] Combining equations (A2) and (A3):

$$-2a_o \int_{r_b}^{r_t} \frac{dr}{\sqrt{(n(r)r)^2 - a_o^2}} \frac{d\ln n}{dr} = -2a_o \int_{a_o}^{a_s} \frac{da}{\sqrt{a^2 - a_o^2}} \frac{d}{da}(\ln n_a - \ln n) \tag{A4}$$

[61] The integral in the right-hand side can be easily inverted to yield

$$\frac{1}{\pi}\int_{a_o}^{a_s} da \frac{-2a}{\sqrt{a^2 - a_o^2}} \int_{r_b}^{r_t} \frac{dr}{\sqrt{(n(r)r)^2 - a^2}} \frac{d\ln n}{dr} = [\ln n_a(a_o) - \ln n(a_o)] - [\ln n_a(a_s) - \ln n(a_s)] \tag{A5}$$

which can be rewritten as

$$\ln \frac{n(a_o)}{n(a_s)} = \ln \frac{n_a(a_o)}{n_a(a_s)} - \tilde{I}_d(a_o) \tag{A6}$$

where a_s is the impact parameter corresponding to the top and bottom of the duct, i.e., $a_s = n(r_t)\, r_t = n(r_b) r_b$, and $\tilde{I}_d$ is given by

$$\tilde{I}_d = \frac{1}{\pi}\int_{a_o}^{a_s} da \frac{-2a}{\sqrt{a^2 - a_o^2}} \int_{r_b}^{r_t} \frac{dr}{\sqrt{(n(r)r)^2 - a^2}} \frac{d\ln n}{dr} = -\frac{2}{\pi}\int_{r_b}^{r_t} dr\, \frac{d\ln n}{dr} \tan^{-1}\left[\frac{a_s^2 - a_o^2}{(n(r)r)^2 - a_s^2}\right]^{1/2} \tag{A7}$$

[62] In terms of refractivity, $\ln n \approx 10^{-6} N$,

$$N(a_o) = N_a(a_o) + [N(r_b) - N(r_t)] - I_d(a_o) \tag{A8}$$

where $N(a_s) = N(r_b)$ and $N_a(a_s) = N(r_t)$ are used and $I_d(a_o) = 10^6\, \tilde{I}(a_o)$.

[63] So far, no approximation (other than $N \ll 1$) has been made.

[64] To evaluate the integral in (A7) analytically, a reasonable approximation can be made where $n(r)$ is bilinear between r_t and r_b (as in Figure 2). It can be shown that

$$I_d = \frac{2}{\pi}(\Delta N)\left[\left(u^2 + 1\right)\tan^{-1} u + u - \frac{\pi}{2}u^2\right] \tag{A9}$$

where $u = \sqrt{(a_s - a_o)/(a_m - a_s)}$. When $u = 0$ ($a_o = a_s$), $I_d = 0$. Thus $N_a(a_s) = N(a_s) - \Delta N$. When $u \gg 1$ (i.e., $a_s - a_o$ being much greater than the thickness of the duct), the term in the bracket in equation (A9) approaches $\pi/2$, which gives $I_d \approx \Delta N$. Thus $N_a(a_o) = N(a_o)$ when a_o is sufficiently far below the duct.

[65] Relations similar to equations (A8) and (A9) have been derived independently by *Xie et al.* [2006], where the expressions are given in terms of height instead of refractivity.

[66] **Acknowledgments.** This work was carried out at the Jet Propulsion Laboratory, California Institute of Technology, under a contract with the National Aeronautics and Space Administration. This work benefited from helpful discussions with Tony Mannucci (JPL), Rob Kursinski (University of Arizona), and Feiqin Xie (University of Arizona).

References

Ahmad, B., and G. L. Tyler (1998), The two-dimensional resolution kernel associated with the retrieval of ionospheric and atmospheric refractivity profiles by Abelian inversion of radio occultation phase data, *Radio Sci.*, *33*(1), 129–142.

Ao, C. O., T. K. Meehan, G. A. Hajj, A. J. Mannucci, and G. Beyerle (2003), Lower troposphere refractivity bias in GPS occultation retrievals, *J. Geophys. Res.*, *108*(D18), 4577, doi:10.1029/2002JD003216.

Beyerle, G., M. E. Gorbunov, and C. O. Ao (2003), Simulation studies of GPS radio occultation measurements, *Radio Sci.*, *38*(5), 1084, doi:10.1029/2002RS002800.

Born, M., and E. Wolf (1999), *Principles of Optics*, 7th ed., Cambridge Univ. Press, New York.

Gorbunov, M. E. (2002), Canonical transform method for processing radio occultation data in the lower troposphere, *Radio Sci.*, *37*(5), 1076, doi:10.1029/2000RS002592.

Gorbunov, M. E., H.-H. Benzon, A. S. Jensen, M. S. Lohmann, and A. S. Nielsen (2004), Comparative analysis of radio occultation processing approaches based on Fourier integral operators, *Radio Sci.*, *39*, RS6004, doi:10.1029/2003RS002916.

Gossard, E. E., and R. G. Strauch (1983), *Radar Observation of Clear Air and Clouds*, Elsevier, New York.

Hajj, G. A., C. O. Ao, B. A. Iijima, D. Kuang, E. R. Kursinski, A. J. Mannucci, T. K. Meehan, L. J. Romans, M. de la Torre Juarez, and T. P. Yunck (2004), CHAMP and SAC-C atmospheric occultation results and intercomparisons, *J. Geophys. Res.*, *109*, D06109, doi:10.1029/2003JD003909.

Ishimaru, A. (1978), *Wave Propagation and Scattering in Random Media*, Elsevier, New York.

Jensen, A. S., M. S. Lohmann, H. Benzon, and A. S. Nielsen (2003), Full spectrum inversion of radio occultation signals, *Radio Sci.*, *38*(3), 1040, doi:10.1029/2002RS002763.

Kursinski, E. R., G. A. Hajj, J. T. Schofield, R. P. Linfield, and K. R. Hardy (1997), Observing Earth's atmosphere with radio occultation measurements using the Global Positioning System, *J. Geophys. Res.*, *102*(D19), 23,429–23,465.

Palmer, P. I., J. J. Barnett, J. R. Eyre, and S. B. Healy (2000), A nonlinear optimal estimation inverse method for radio occultation measurements of temperature, humidity, and surface pressure, *J. Geophys. Res.*, *105*(D13), 17,513–17,526.

Patterson, W. L. (1982), Climatology of marine atmospheric refractive effects: A compendium of the Integrated Refractive Effects Prediction System (IREPS) historical summaries, *Tech. Rep. 573 (ADA155241)*, Nav. Ocean Syst. Cent., San Diego, Calif.

Purves, C. P. (1974), Geophysical aspects of atmospheric refraction, *NRL Rep. 7725 (AD0780433)*, Nav. Res. Lab., Washington, D. C.

Smith, E. K., and S. Weintraub (1953), The constants in the equation for atmospheric refractive index at radio frequencies, *Proc. IRE*, *41*, 1035–1037.

Sokolovskiy, S. V. (2001), Tracking tropospheric radio occultation signals from low Earth orbit, *Radio Sci.*, *36*(3), 483–498.

Sokolovskiy, S. (2003), Effect of superrefraction on inversions of radio occultation signals in the lower troposphere, *Radio Sci.*, *38*(3), 1058, doi:10.1029/2002RS002728.

Solheim, F. S., J. Vivekanandan, R. H. Ware, and C. Rocken (1999), Propagation delays induced in GPS signals by dry air, water vapor, hydrometeors, and other particulates, *J. Geophys. Res.*, *104*(D8), 9663–9670.

von Engeln, A., and J. Teixeira (2004), A ducting climatology derived from the European Centre for Medium-Range Weather Forecasts global analysis fields, *J. Geophys. Res.*, *109*, D18104, doi:10.1029/2003JD004380.

von Engeln, A., G. Nedoluha, and J. Teixeira (2003), An analysis of the frequency and distribution of ducting events in simulated radio occultation measurements based on ECMWF fields, *J. Geophys. Res.*, *108*(D21), 4669, doi:10.1029/2002JD003170.

von Engeln, A., J. Teixeira, J. Wickert, and S. A. Buehler (2005), Using CHAMP radio occultation data to determine the top altitude of the planetary boundary layer, *Geophys. Res. Lett.*, *32*, L06815, doi:10.1029/2004GL022168.

Wang, L., and M. A. Geller (2003), Morphology of gravity-wave energy as observed from 4 years (1998–2001) of high vertical resolution U. S. radiosonde data, *J. Geophys. Res.*, *108*(D16), 4489, doi:10.1029/2002JD002786.

Xie, F., S. Syndergaard, E. R. Kursinski, and B. M. Herman (2006), An approach for retrieving marine boundary layer refractivity from GPS occultation data in the presence of superrefraction, *J. Atmos. Oceanic Technol.*, *23*, 1629–1644.

Zou, X., B. Wang, H. Liu, R. A. Anthes, T. Matsumura, and Y.-J. Zhu (2000), Use of GPS/MET refraction angles in three-dimensional variational analysis, *Q. J. R. Meteorol. Soc.*, *126*(570), 3013–3040.

C. O. Ao, Jet Propulsion Laboratory, M/S 138-308, 4800 Oak Grove Dr., Pasadena, CA 91109, USA. (chi.o.ao@jpl.nasa.gov)